Zeolite-Catalyzed Isobutene Amination: Mechanism and Kinetics

Christopher R. Ho,[†,§,⊥] Lance A. Bettinson,[†,§,⊥] Jeongmoon Choi,[†] Martin Head-Gordon,[‡,§] and Alexis T. Bell*[,†,§]

[†]Department of Chemical and Biomolecular Engineering University of California, Berkeley, California 94720, United States

[‡]Department of Chemistry University of California Berkeley, California 94720, United States

[§]Chemical Sciences Division Lawrence Berkeley National Laboratory Berkeley, California 94720, United States

ABSTRACT: Amination of isobutene with NH_3 was investigated over Brønsted acidic zeolites at 1 atm and 453−483 K. To compare catalytic activities over different zeolites, the measured reaction rates are normalized by the number of active sites determined by *tert*-butylamine temperature-programmed desorption (TPD). Small- and medium-pore zeolites with one-dimensional channels exhibit low activity because of pore blockage by adsorbed *tert*-butylammonium ions. However, turnover frequencies and activation energies are not sensitive to framework identity, as long as the active site is accessible to isobutene and *tert*-butylamine. Kinetic measurements and FTIR spectroscopy reveal that the Brønsted acid sites in MFI are covered predominantly with *tert*-butylammonium ions under reaction conditions. The desorption of *tert*-butylamine is assisted by the concurrent adsorption of isobutene. DFT simulations show that at very low *tert*-butylamine partial pressures, for example, at the inlet to the reactor, *tert*-butylamine desorption is rate-limiting. However, at sufficiently high *tert*-butylamine partial pressures (>0.03 kPa), protonation of isobutene to the corresponding carbenium ion limits the rate of amination.

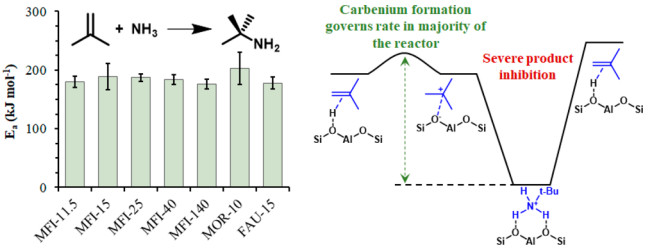

INTRODUCTION

Alkylamines can be synthesized by hydroamination of olefins with NH_3. This process is attractive because olefin feedstocks are readily available, and the atom economy is 100%. However, the reaction is endergonic and entropically disfavored, which limits the commercial scope of the reaction.[1] Because of these difficulties, hydroamination is used industrially only for the conversion of isobutene ($C_4^=$) to *tert*-butylamine (*t*-BuNH_2) in a process commercialized by BASF (Scheme 1).[2] Pentasil zeolites are used as the catalyst and are operated at temperatures and pressures of around 573 K and 300 atm, respectively. Under these conditions the equilibrium conversion is approximately 20−40% depending on the NH_3/isobutene ratio.[2−5] Lower reaction temperatures are desirable because they would enable attainment of higher equilibrium conversions; however, because of the large activation barrier for the reaction (up to 220 kJ mol^{-1}), operation at lower temperatures is not feasible.[6] Therefore, there is a need to understand the mechanism and kinetics of hydroamination and the factors leading to the high apparent activation energy. The issue of whether zeolite composition and structure affect the rate of this reaction also deserves further attention.

Scheme 1. Isobutene Amination to *tert*-Butylamine

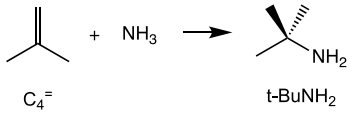

Direct amination of olefins over zeolites was first reported by Deeba et al.[7−9] H-MOR and H-OFF were shown to be active for ethylene amination at 633 K and 52 atm, but the Na-exchanged analogs were not active, highlighting the importance of acid sites.[7] The authors proposed that olefins are protonated by either a Brønsted acid −OH or an adsorbed ammonium ion to form the corresponding carbenium ion, which was thought to be a key intermediate in the reaction. Mizuno et al. have shown that isobutene amination over H-MFI at 473 K and 1 atm is zero order with respect to NH_3 partial pressure and positive order with respect to isobutene partial pressure, leading them to conclude that NH_3 adsorbs more strongly than isobutene under reaction conditions.[10] Lequitte et al. have observed similar kinetics for 1-butene and isobutene amination at 500−600 K and 40 atm.[6] However, these authors postulated that the reaction proceeds through an olefin π-complex intermediate instead of a carbenium ion and hypothesized that coupling of an olefin π-complex and surface ammonium ion is rate-limiting.

A key question regarding the reaction mechanism is whether the product amine influences the reaction rate, which would alter the interpretation of rate data. The heat of adsorption for small-chained alkylamines over zeolites is 50−100 kJ mol^{-1} higher than that of NH_3, suggesting that even small concentrations of amine can inhibit the reaction.[11−14] Lercher and co-workers have studied the amination of alcohols over H-MOR and demonstrated that NH_3-assisted desorption of surface alkylammonium species is much slower than the C−N coupling step.[15,16] This conclusion is supported by temperature-programmed desorption (TPD) studies of alkylamines, which show that alkylamines adsorbed on Brønsted acid sites will decompose to the corresponding olefin and NH_3 instead of desorbing.[13,17,18]

The relationship between zeolite geometry and catalytic activity is also unclear. Mizuno et al. have measured isobutene amination rates over H-MFI as a function of Si/Al ratio and found that rates go through a maximum at a Si/Al ratio of 40.5.[10] They proposed that acid site density and acid strength were both critical factors for the reaction. Gao et al. have observed a similar dependence between isobutene conversion and Si/Al ratio; however, they interpreted their findings on the basis of variations in Brønsted acid site density.[19] The framework also appears to play an important role in the reaction. For a given Si/Al ratio, large differences in the reaction rate and activation energy are observed depending on the framework.[6,10,19] Small-pored zeolites are inactive because *t*-$BuNH_2$ is too bulky to fit within the pores. However, the effect of pore geometry and connectivity on the turnover frequency has not been established. Furthermore, to the best of our knowledge, quantitative measurements of the active site density as a function of Si/Al ratio and framework structure have not been performed in the context of amination reactions.

The aim of this work is to clarify the mechanism of isobutene amination and identify key structural properties responsible for catalytic activity. We show that zeolites with only 8- and 10-membered rings are active only if they possess a multidimensional pore structure, which precludes complete clogging due to *t*-$BuNH_2$ adsorption. Beyond that, there is little influence of pore size and geometry on the intrinsic rate over a Brønsted acid site, provided the site is accessible. *t*-$BuNH_2$ is the predominant surface species, and its desorption is assisted by the concurrent adsorption of isobutene. Protonation of isobutene to the carbenium ion is rate-limiting in the majority of the reactor, and the subsequent coupling with NH_3 occurs rapidly in a virtually barrierless step.

EXPERIMENTAL METHODS

Catalyst Synthesis. MFI (Zeolyst), FAU (Zeolyst), and MOR (Süd-Chemie) samples were obtained commercially in their NH_4^+ forms. SFV, MWW, and TON were synthesized by Chevron Energy Technology, Co. (Richmond, CA).[20] FER (Tosoh) was obtained in the K^+ form. To convert FER to the NH_4^+ form, 0.3 g of K-FER was stirred in a 100 mL solution of 1 M NH_4NO_3 for 24 h at 298 K. The resulting slurry was washed and filtered in H_2O. Commercial zeolite samples in this work are designated by their framework identity and nominal Si/Al ratio. For example, MFI-15 represents an MFI sample with a Si/Al ratio of 15 as reported by the manufacturer. The H^+ forms of all zeolites were obtained by calcination of the NH_4^+ forms in 100 mL min^{-1} of air at 773 K for 4 h.

Characterization Techniques. The Si/Al ratio was determined by elemental analysis carried out by Galbraith Laboratories using ICP-OES. Infrared spectra (FTIR) were acquired using a Thermo Scientific Nicolet 6700 spectrometer equipped with a liquid-nitrogen-cooled MCT detector. Samples were prepared by pressing ∼0.04 g of catalyst into a 20 mm-diameter pellet and placing it into a custom-built transmission cell with CaF_2 windows. All pellets for FTIR were pretreated in helium at 773 K for 1 h before measurement. Isobutene and NH_3 were fed into the transmission cell through mass flow controllers, and *t*-$BuNH_2$ was introduced into the cell in 1 μL doses through an injection port using a syringe.

NH_3-TPD measurements were performed in a custom-built unit equipped with an MKS Cirrus mass spectrometer. In a typical experiment, 0.2 g of sample was loaded into a quartz-tube, packed-bed reactor and held in place with quartz wool. The sample was pretreated in 30 mL min^{-1} of He for 20 min at 773 K before cooling to 433 K. Afterward, 5 mL min^{-1} of NH_3 and 300 mL min^{-1} of He were introduced for 1 h to saturate the sample. The sample was subsequently treated in 300 mL min^{-1} of He for 15 h to purge any physisorbed NH_3. The TPD measurement was conducted using a flow of 300 mL min^{-1} of He and 0.5 mL min^{-1} of Ar, which served as an internal standard to correct for any drift in signal. Once the baseline was stable, the temperature was ramped to 973 K at a rate of 5 K min^{-1}. Calibration of the m/z = 17 (NH_3, OH) signal was performed before and after every TPD measurement by flowing known concentrations of NH_3 and Ar into the mass spectrometer. The contribution of water to the m/z = 17 signal was accounted for by measuring the water concentration from the m/z = 18 signal and noting the relative signal intensities of m/z = 17 and 18 when only water is present.

A similar procedure was used for *t*-$BuNH_2$-TPD studies. After an identical pretreatment in He, the sample was cooled to 423 K. *t*-$BuNH_2$ (0.16 mL h^{-1}) was volatilized in 300 mL min^{-1} of He using a syringe pump (World Precision Instruments, SP100I) and fed over the sample for 1 h. After the sample was purged in He for 15 h, the TPD measurement was performed by ramping the temperature to 973 K at a rate of 5 K min^{-1}. The NH_3 signal (m/z = 17) was used to determine the rate of *t*-$BuNH_2$ decomposition because the isobutene signal (m/z = 41) could not be quantified due to additional cracking and oligomerization of isobutene.

Measurements of Catalytic Activity. Measurements of reaction rates were carried out using a quartz-tube, packed-bed reactor (10 mm inner diameter). Quartz wool was placed below the catalyst bed to hold the catalyst in place. The reactor temperature was maintained using a tube furnace equipped with a Watlow temperature controller and a K-type thermocouple. Prior to reaction, the catalyst was treated in 30 mL min^{-1} of H_2 at 773 K for 2 h before cooling to the reaction temperature. Liquid reactants, such as propylamine and *t*-$BuNH_2$, were volatilized into an isobutene and NH_3 feed stream using a syringe pump. All experiments were carried out at atmospheric pressure. Product streams were analyzed by gas chromatography using an Agilent 6890A GC fitted with a HP-5 capillary column (30 m × 0.32 mm × 0.25 μm) and a flame ionization detector.

Density Functional Theory QM/MM Calculations. To gain further insights into the amination mechanism, density functional theory (DFT) calculations were carried out for proposed reaction pathways. A QM/MM (quantum mechanics/molecular mechanics) model was used to represent the

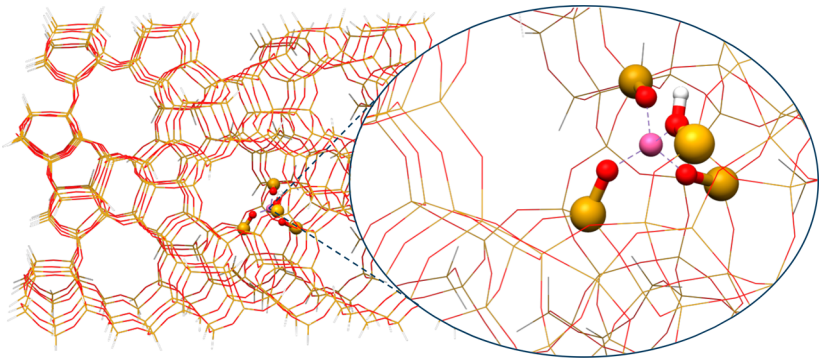

Figure 1. QM/MM model for H-MFI (T5-T437). Atoms in yellow, red, white, and pink represent Si, O, H, and Al atoms, respectively. Spherical atoms represent the QM region. All other atoms comprise the MM region.

zeolite-reactant system.[21,22] Figure 1 illustrates the T442 H-MFI cluster used for this work. The adsorbates and a 5 tetrahedral atom (T5) cluster representing the Brønsted acid site (presumed to be associated with an Al atom located at the T12 position in the zeolite) were described quantum mechanically. The extended zeolite structure comprised 437 tetrahedral Si atoms surrounding this site, with hydrogen atoms replacing terminal oxygen atoms. This region was described by molecular mechanics using a CHARMM force field.[23] Geometry optimizations and transition state searches were performed at the ωB97X-D/6-31+G** level of theory; only the QM region was relaxed, whereas all of the atoms in the MM region were held fixed at their crystallographic positions. Vibrational analysis was performed at the same level of theory, while single-point energy calculations were performed at the ωB97X-D/6-311++G(3df,3pd) level of theory. Entropies were determined by considering zero point vibrational and temperature corrections using the quasi-RRHO approach, which replaces low-frequency (<100 cm^{-1}) vibrational entropy contributions with an interpolation between vibrational and free-rotor rotational values.[24] This approach was extended to calculate the enthalpies of adsorbates, as previously recommended for H-MFI.[22] All calculations were performed using the Q-Chem software package.[25] Following identification and subsequent thermal correction of all intermediate and transition state geometries, the kinetics of the reaction were analyzed using the energetic span model considering reactant and product partial pressures.[26]

RESULTS AND DISCUSSION

Effects of Zeolite Structure and Composition on Isobutene Amination. The apparent rate constants were measured over a variety of zeolites, and the results are shown in Figure 2. The rates are normalized per Brønsted acid site as measured by NH_3-TPD. For FAU, the Brønsted acid site density could not be measured by NH_3-TPD because of the overlap of desorption features associated with Brønsted and Lewis acid sites. Thus, the H^+/Al ratio in FAU was estimated to be 1 based on the lack of O−H stretching frequencies associated with extra-framework Al atoms, as measured by FTIR.[27] Rate constants were determined using eq 1.

$$r_{app} = \frac{k_{app}[C_4^=]}{[t\text{-BuNH}_2]_f} \quad (1)$$

In this expression, k_{app} represents an apparent rate constant, and $[t\text{-BuNH}_2]_f$ represents the concentration of t-$BuNH_2$ at the outlet of the reactor. The justification for using this expression is discussed below. The results presented in Figure 2 are very similar to those reported by Mizuno et al. and Gao et al., the activity per Brønsted acid site decreasing in the order of MFI > MWW > MOR > FAU > FER.[10,19]

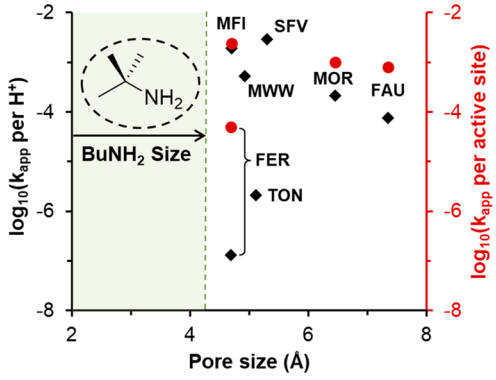

Figure 2. Apparent rate constants normalized per Brønsted acid site (black diamonds) or active site (red circles) plotted as a function of the diameter of the largest sphere that could diffuse through the zeolite as determined by Foster et al.[29] T = 473 K; P = 1 atm; $P_{C_4^=}$ = 32 kPa; P_{NH_3} = 69 kPa; total gas flow rate at STP = 20−50 mL min^{-1}.

To make a more accurate comparison of catalytic activity, the measured rates must be normalized by the number of active sites. Although Brønsted acidic protons have been identified as the active site for alkene amination in zeolites, not all protons may be accessible. This is especially true in the case of small-pored zeolites, where the size of the micropores restricts the formation of a product or transition state. Thus, prior studies that report amination rates normalized per Brønsted acid site underestimate the intrinsic activity.[10,28]

To choose the appropriate technique for measuring the density of active sites for amination, it is helpful to consider the reverse reaction, in which an alkylamine decomposes to form NH_3 and the corresponding olefin. This Hofmann elimination reaction (also known as deamination) proceeds through an alkylammonium intermediate, which adsorbs strongly on Brønsted acid sites (ΔH_{ads} = 200−250 kJ mol^{-1}).[12,14,30−32] In fact, the adsorption strength is so large that alkylammonium ions will preferentially undergo Hofmann elimination at elevated temperatures instead of desorbing. The number of active sites for Hofmann elimination can be determined from alkylamine TPD by measuring the amount of decomposition products formed. Since the number of active sites for Hofmann elimination and olefin amination are equivalent by the

principle of microscopic reversibility, alkylamine TPD can also be used to determine the density of active sites for amination.

To determine the fraction of Brønsted acid sites that are catalytically active, NH_3-TPD and *t*-$BuNH_2$-TPD were conducted over MFI, MOR, FAU, and FER. A typical *t*-$BuNH_2$-TPD profile is shown in Figure 3. The *t*-$BuNH_2$

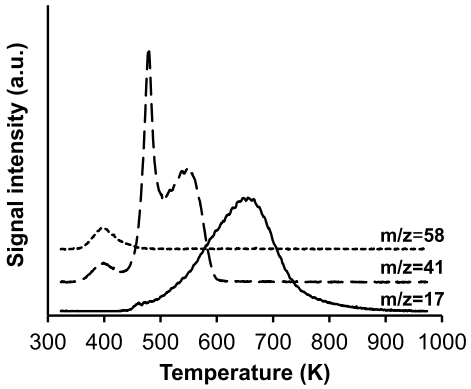

Figure 3. *t*-$BuNH_2$-TPD study over MFI-15. Desorption profiles have been offset for clarity. The m/z values are assigned as follows: m/z = 58, *tert*-butylamine; m/z = 41, isobutene, m/z = 17, ammonia.

desorption peak (m/z = 58) around 400 K corresponds to physisorbed species that bind weakly to silanol groups or extra-framework Al atoms. *tert*-Butylammonium ions adsorbed on Brønsted acid sites decompose into isobutene and NH_3 at around 523 K. Two desorption peaks at m/z = 41 are observed. These likely correspond to the immediate desorption of isobutene and subsequent oligomerization and cracking to other hydrocarbons.[17] NH_3 remains on the surface up to ~673 K due to strong interactions with the framework.

The NH_3 desorption profiles for NH_3-TPD and *t*-$BuNH_2$-TPD are shown in Figure 4 for various zeolites. The NH_3-TPD method used here has been shown to accurately measure the number of Brønsted acid sites in MFI.[33,34] However, for large pore zeolites, such as FAU, NH_3-TPD cannot adequately distinguish between Brønsted acid protons adjacent to framework Al atoms and Lewis acid sites from the extra-framework Al species.[35] The NH_3 desorption temperature varies with framework (FAU < MFI < FER ~ MOR). However, no conclusions can be drawn about relative acid strengths since NH_3 desorption temperature is also influenced by particle size and site density.[13,36] For FAU and MFI, the amount of desorbed NH_3 in the NH_3-TPD and *t*-$BuNH_2$-TPD is identical, which indicates that all Brønsted acid sites are active for amination, as shown in Table 1. On the other hand, for MOR and FER, the active site densities as measured by *t*-$BuNH_2$-TPD are lower than the corresponding Brønsted acid site densities measured by NH_3-TPD. For these frameworks, some of the acid sites are inaccessible because they are located in voids that are too small to accommodate *t*-$BuNH_2$ (end-to-end diameter = 4.3 Å).

The apparent rate constants and activation energies for each zeolite are presented in Table 1. The activation energy over FER could not be measured due to its very low activity. The apparent rate constants determined for all zeolites are within a factor of 3 except for FER. We hypothesize that the slightly lower activities over MOR and FAU are due to the larger pore sizes, which result in a lower electrostatic stabilization of the transition state. It is interesting to note that even after amination rates have been normalized by the number of active sites, the catalytic activity of FER is roughly 50 times lower than that for the other samples. This is likely due to the 1-D structure of the 10-MR channels. Since the 8-MRs are too small to accommodate *t*-$BuNH_2$, the product can only diffuse through the 10-MR channels. As shown in the *t*-$BuNH_2$-TPD studies, *t*-$BuNH_2$ binds strongly to the active site. *t*-$BuNH_2$ adsorption near the pore mouths would impede diffusion of the reactant toward the interior of the zeolite and drastically lower the reaction rate. This same effect is also observed for TON (Figure 2), whose pore topology only consists of 1-D channels.

For zeolites with larger pores (MFI, MOR, FAU), the activation energy is invariant with structure. This finding is inconsistent with what Lequitte et al. have reported.[6] However, those authors determined activation energies based on the temperature dependence of *t*-$BuNH_2$ yield, which is influenced by the degree of product inhibition. In this work, the reported activation energies were determined by measuring rate constants as a function of temperature, which account for the inherent kinetics of the reaction. Rate constants over MFI-11.5, MOR-10, and FAU-15 are also within error of each other, suggesting that all active sites possess similar reactivity. The variations in rate for MFI samples with different Si/Al ratios (k_{app} = 0.9 × 10^{-3} to 2.9 × 10^{-3} h^{-1}) indicate that the environment around the active site has a relatively small influence on its catalytic activity. However, these effects are not as significant as those due to site accessibility. To gain a more detailed understanding of the site requirement and reaction mechanism, MFI was chosen for additional investigation because of its high thermal stability and catalytic activity.

Kinetics of Isobutene Amination over MFI. The conversion of isobutene to *t*-$BuNH_2$ over MFI-15 is shown in Figure 5. No deactivation was observed after 5 h. The initial

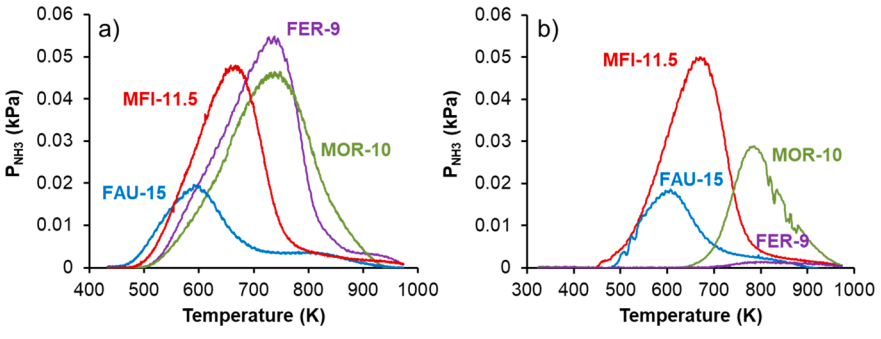

Figure 4. Ammonia desorption during (a) NH_3-TPD and (b) *t*-$BuNH_2$-TPD for various zeolites.

Table 1. Properties of Zeolite Catalysts and Their Activities for Isobutene Amination

catalyst	supplier	Si/Al ratio	H^+/Al_{tot} ratio[b]	active site/H^+ ratio[c]	active site density[c] (mmol/g)	k_{app}[d] ($\times 10^{-3}$ mol (mol active site)$^{-1}$ h^{-1})	activation energy (kJ mol^{-1})
MFI-11.5	Zeolyst (CBV-2314)	12.1[a]	0.86	~1	1.08	0.9 ± 0.2	180 ± 10
MFI-15	Zeolyst (CBV-3024E)	16.5[a]	0.73	~1	0.62	2.4 ± 0.3	189 ± 22
MFI-25	Zeolyst (CBV-5524G)	28.8[a]	0.75	~1	0.42	2.9 ± 0.4	187 ± 7
MFI-40	Zeolyst (CBV-8014)	43.7[a]	0.70	~1	0.31	2.6 ± 0.6	184 ± 8
MFI-140	Zeolyst (CBV-28014)	142[a]	0.69	~1	0.09	1.5 ± 0.2	176 ± 8
MOR-10	Süd-Chemie (NH4-MOR20)	10.8	0.90	0.41	0.48	1.0 ± 0.3	203 ± 28
FAU-15	Zeolyst (CBV720)	14.4			0.42	0.81 ± 0.09	178 ± 10
FER-9	Tosoh (HSZ-720 KOA)	8.4[a]	0.73	0.03	0.03	0.05 ± 0.02	-

[a]Data taken from Janda et al.[20,37] [b]Determined from NH_3-TPD studies. [c]Determined from t-$BuNH_2$-TPD studies. [d]Reaction conditions: T = 473 K; P = 1 atm; H-MFI-16.5 = 0.02 g; $P_{C_4^=}$ = 32 kPa; P_{NH_3} = 69 kPa.

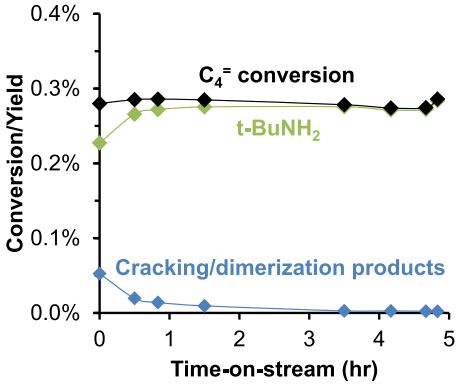

Figure 5. Time-on-stream study of isobutene amination over MFI-15. T = 473 K; P = 1 atm; H-MFI-16.5 = 0.02 g; $P_{C_4^=}$ = 32 kPa; P_{NH_3} = 69 kPa; total gas flow rate at STP = 20 mL min^{-1}.

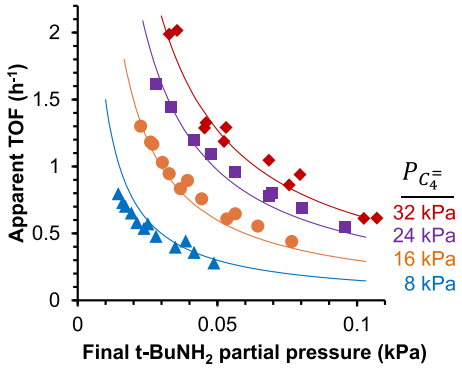

Figure 6. Apparent turnover frequencies over MFI-15 as a function of the final partial pressure of t-$BuNH_2$ at various isobutene partial pressures. Solid lines represent the fitted kinetic model shown in eq 1. T = 473 K; P = 1 atm; P_{NH_3} = 69 kPa; WHSV = 5–96 h^{-1}.

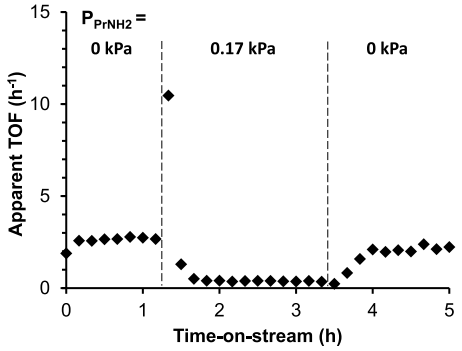

Figure 7. Effect of cofeeding propylamine on amination rates over MFI-15. T = 473 K; P = 1 atm; P_{NH_3} = 69 kPa; m_{cat} = 0.01 g.

selectivity to t-$BuNH_2$ was 81% and increased to >99% with increasing time-on-stream. Side products due to isobutene cracking and oligomerization were observed only at short time-on-stream (<2 h). Both of these reactions are catalyzed by Brønsted acid sites on H-MFI.[37] Under reaction conditions, these sites are gradually passivated by adsorbed NH_3 or t-$BuNH_2$, leading to a transient decay in the rates of cracking and oligomerization.

Space-time studies were conducted under steady-state conditions. The t-$BuNH_2$ formation rate at 473 K is nonlinear with respect to space time for a range of isobutene conversions ($X_{C_4^=}$ = 0.07–0.4%). The equilibrium conversion under these conditions is approximately 2–3%,[5,10] well above the values observed in the space-time study. This indicates that the nonlinearity in reaction rate with respect to space time is not due to an approach to equilibrium. Instead, the reaction appears to be inhibited by the t-$BuNH_2$ product. To understand the effects of t-$BuNH_2$ inhibition, apparent turnover frequencies (TOF) were plotted as a function of the final t-$BuNH_2$ partial pressure. The fitted curve in Figure 6 is not concave downward, which is further evidence that reaction rates are not limited by an approach to equilibrium. For a given isobutene partial pressure, the apparent TOF is inversely proportional to the final t-$BuNH_2$ partial pressure (Figure 6), suggesting that there is severe product inhibition due to competitive adsorption of t-$BuNH_2$.

To understand the magnitude of amine inhibition, n-propylamine was cofed into the reactor after reaching steady-state (Figure 7). Upon introduction of propylamine, an initial pulse of t-$BuNH_2$ was observed. The reaction rate subsequently decayed until it reached one-eighth of its original value. Although the propylamine partial pressure (0.17 kPa) was 400 times lower than that of NH_3 (69 kPa), propylamine titrated a majority of the active sites. This is due to the stronger basicity of propylamine compare to NH_3. Indeed, micro-calorimetry studies by Parillo et al. have shown that alkylamines bind to protons in MFI more strongly than NH_3 by 50–100 kJ mol^{-1}.[13,14] For the range of reaction conditions tested, the final t-$BuNH_2$ partial pressure is between 0.01–0.15 kPa, which is similar to the propylamine partial pressure used in the experiment. These results provide further evidence that the actives sites are saturated with adsorbed t-$BuNH_2$, even at isobutene conversions below 1%.

Initial rate studies were performed to determine the rate dependence on isobutene and NH_3 partial pressures at a given total flow rate. The reaction is zero order with respect to NH_3 (Figure 8). Since the active sites are covered predominantly by

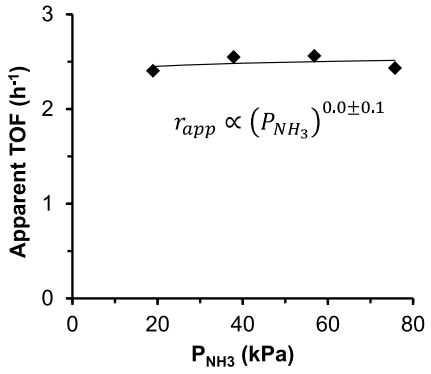

Figure 8. Effect of NH_3 partial pressure on amination rates over MFI-15. T = 473 K; P = 1 atm; $P_{C_4^=}$ = 32 kPa; m_{cat} = 0.01 g.

adsorbed t-BuNH_2, the zero-order dependence indicates that NH_3 is not involved in the rate-limiting step (RLS) or any step prior to the RLS. More specifically, these results show that C−N coupling between isobutene and NH_3 cannot be the RLS.

The amination rate appears to be 0.7 order with respect to isobutene (Figure S2), which is similar to what Mizuno et al. have reported ($r \propto P_{C_4^=}^{0.8\pm0.1} P_{NH_3}^{0\pm0.1}$).[10] However, changes in the isobutene partial pressure at a given total flow rate affect the final t-BuNH_2 partial pressure, which also has a strong influence on the rate. To obtain the intrinsic rate dependence on isobutene partial pressure, a series of space time studies were conducted at different isobutene partial pressures (Figure 6). It has already been shown that the apparent rate is inverse order with respect to t-BuNH_2 partial pressure and zero order with respect to NH_3 partial pressure. Thus, if the product of the apparent rate and final t-BuNH_2 partial pressure is plotted against the isobutene partial pressure, the rate order can be determined from a power law fit. Figure 9 shows that the apparent rate is first order with respect to isobutene after correcting for the inhibition by t-BuNH_2, suggesting that the RLS only involves isobutene.

The activation energy over MFI is invariant with the Si/Al ratio, at least within measurement error (Table 1). However,

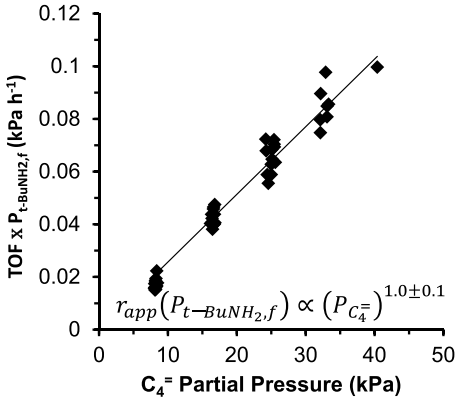

Figure 9. Effect of cofeeding propylamine on amination rates over MFI-15. T = 473 K; P = 1 atm; $P_{C_4^=}$ = 32 kPa.

the rate constants for MFI-11.5 and MFI-140 are significantly lower than that of MFI-15, MFI-25, and MFI-40, even after rates have been normalized per active site. This suggests that there are slight variations in the reactivity of an active site, which may depend on its location and surrounding environment. For example, MFI samples with lower Si/Al ratios tend to have a higher fraction of proton site pairs for which their corresponding Al framework atoms are either next-nearest neighbors or next-next-nearest neighbors.[34,37] To determine where these proton site pairs exhibit different activity compared to isolated H^+ sites, reaction rates were normalized by the number of paired sites as determined by cobalt titration studies performed by Janda et al.[37] and plotted as a function of the Si/Al ratio (Figure 10). If paired sites were much more

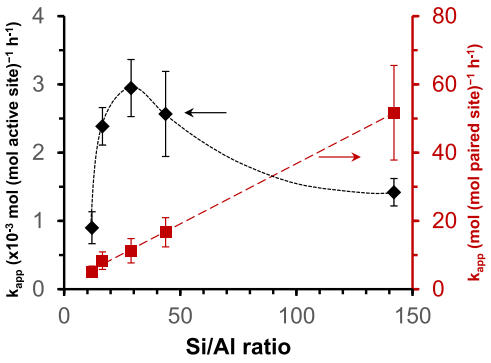

Figure 10. Apparent rate constants for isobutene amination over MFI as a function of Si/Al ratio. Rate constants have either been normalized by the number of measured active sites or number of paired sites. T = 473 K; P = 1 atm; P_{NH_3} = 69 kPa.

reactive than isolated sites, the turnover per paired site should be invariant with Si/Al ratio. Instead, a large systematic difference in rate per paired sites is observed with respect to Si/Al ratio, suggesting that paired sites are not the principal sites involved in isobutene amination.

Another possibility is that differences in active site location is responsible for the differences in observed rate. The importance of active site location has been demonstrated for other zeolite-catalyzed reactions such as alkane dehydrogenation and cracking.[38] For MFI with a Si/Al ratio between 12 and 44, Janda et al. have shown that the fraction of paired sites in straight and sinusoidal channels tend to increase with increasing Si/Al.[37] However, determining the locations of all active sites experimentally is difficult due to the complex geometric structure of MFI.[39,40] Thus, further conclusions about reactivity differences due to active site location cannot be made. Regardless, the observed variations in rates over MFI correspond to a variation in $\Delta G^{\ddagger}$ of only 5 kJ mol^{-1}, which highlights that all Brønsted acid sites have similar activities as long as the sites are accessible to the reactants and product.

Mechanism of Isobutene Amination over H-MFI. On the basis of the dependencies of the rate of isobutene amination on partial pressures of isobutene, NH_3, and t-BuNH_2, we hypothesize that activation of adsorbed isobutene to the corresponding carbenium ion is the RLS. Several observations support this hypothesis. The formation of the carbenium ion is known to be catalyzed by strong Brønsted acid sites in MFI, and sodium titration of these acid sites renders the catalyst inactive for t-BuNH_2 formation.[7,8] The stability of the carbenium also depends on the degree of

branching in the olefin. Tertiary carbocations are more stable than secondary carbocations, which in turn are more stable than primary carbocations. When the reaction was performed with propene instead of isobutene, no products were detected (data not shown), consistent with DFT calculations by Cnudde et al. showing that formation of a secondary carbenium is thermodynamically unfavorable on H-MFI.[41] In addition, Song et al. have observed the carbenium ion of 1,3-dimethylcyclopentene in H-MFI using ^{13}C CP/MAS NMR and have shown that these carbenium cations are converted to alkylamines upon exposure to NH_3.[42]

In situ FTIR spectroscopy was used to probe the identity of surface intermediates under reaction conditions (Figure 11).

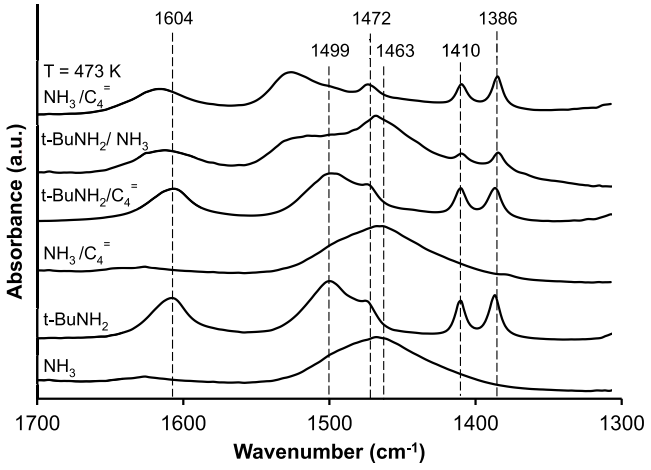

Figure 11. FTIR difference spectra of MFI-15 taken 1 h after introduction of isobutene, NH_3, or *t*-$BuNH_2$. Spectra were taken at 433 K unless otherwise specified.

NH_3 adsorption on MFI gives rise to a broad feature at 1463 cm^{-1} due to the bending mode of NH_4^+ species. When NH_3 (69 kPa) and isobutene (32 kPa) are cofed over MFI at 393 K, the feature at 1463 cm^{-1} is unperturbed and no C−H bending modes are detected, consistent with an NH_3-saturated surface. Similarly, when 1 μL of *t*-$BuNH_2$ is introduced into a pure isobutene feed over MFI at 393 K, the C−H (1472, 1386, 1410 cm^{-1}) and N−H (1604, 1499 cm^{-1}) deformation modes of *tert*-butylammonium ions are unperturbed by the presence of isobutene. However, when *t*-$BuNH_2$ and NH_3 are fed over MFI at 393 K, the N−H deformation modes are blue-shifted to 1620 and 1530 cm^{-1}, showing that NH_3 can interact with the N−H bonds of *tert*-butylammonium ions, likely through hydrogen-bonding interactions (Figure 11). However, this interaction is weak, as NH_3 completely desorbs from the surface after several minutes once the flow of NH_3 is halted (Figure S3).

An important element of the reaction mechanism is the manner in which *t*-$BuNH_2$ desorbs from the zeolite surface. As illustrated by *t*-$BuNH_2$-TPD, *t*-$BuNH_2$ does not desorb molecularly from the surface, suggesting that desorption by some other mechanism must occur. For example, interactions with NH_3 or isobutene could aid *t*-$BuNH_2$ desorption by facilitating N−H bond cleavage of the *tert*-butylammonium ion and stabilizing the resulting Brønsted acid proton. Indeed, Veefkind et al. have shown that NH_3 mediates the desorption of alkylamines for alcohol amination in mordenite at 633 K.[16] However, *t*-$BuNH_2$ does not desorb at 433 K even in the presence of NH_3, as shown in Figure 10. To probe the desorption mechanism further, a sample of MFI-15 was saturated with *t*-$BuNH_2$, followed by introduction of NH_3 (1.7 kPa) at 423 K. An initial pulse of *t*-$BuNH_2$ was observed in the outlet stream (Figure 12a), and the quantity desorbed (0.3 mmol g_{cat}^{-1}) was equivalent to the amount of physisorbed amine as measured by *t*-$BuNH_2$-TPD in He (Figure 12b). However, no *t*-$BuNH_2$ was detected during subsequent TPD in NH_3 flow, which is further evidence that NH_3 displaces physisorbed *t*-$BuNH_2$ but not strongly bound *tert*-butylammonium ions on Brønsted acid sites. NH_3 also has no effect on the decomposition temperature of *t*-$BuNH_2$ (Figure 12c), consistent with FTIR observations of a weak interaction between NH_3 and *tert*-butylammonium ions. Although the m/z = 41 signal during *t*-$BuNH_2$-TPD is lower when performed in an NH_3/He atmosphere instead of pure He, it is difficult to interpret the meaning of this difference, as other hydrocarbons formed due to cracking and oligomerization of isobutene also contribute to the signal.

In summary, FTIR and *t*-$BuNH_2$-TPD measurements show that *t*-$BuNH_2$ does not desorb from MFI near reaction temperatures, even in the presence of NH_3 or isobutene. While it is possible that isobutene or NH_3 can temporarily displace the surface *tert*-butylammonium ions, the reverse reaction is much more rapid at sufficient *tert*-butylamine partial pressures, and *t*-$BuNH_2$ will readsorb before it can diffuse out of the zeolite. However, if a transiently adsorbed isobutene species reacts with NH_3 before *t*-$BuNH_2$ can readsorb, then another *tert*-butylammonium ion will form on the surface and the catalytic cycle can continue. Thus, while displacement of *tert*-butylammonium ions by isobutene is the most energetically uphill step in the reaction, the activation of isobutene to the corresponding carbenium ion controls the speed of catalytic turnover, and hence is the RLS. This proposed mechanism is

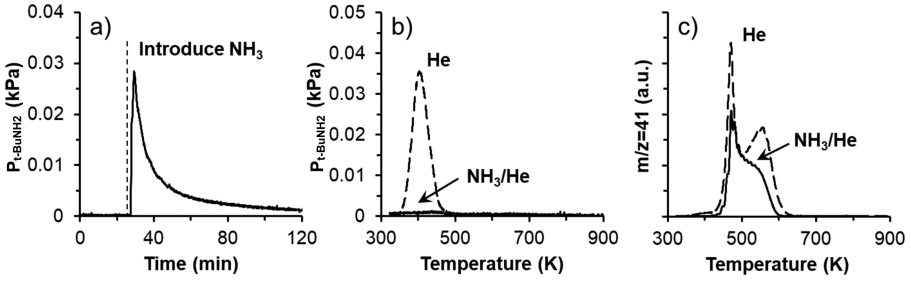

Figure 12. *t*-$BuNH_2$-TPD over MFI-15 in the presence or absence of NH_3 flow. (a) *t*-$BuNH_2$ desorption at 423 K after introduction of NH3. (b) *t*-$BuNH_2$ TPD profile in either He or NH_3/He flow. (c) Signal intensity of m/z = 41 (isobutene + other hydrocarbons) during *t*-$BuNH_2$-TPD in either He or NH_3/He flow.

illustrated in Scheme 2, where k_2 is the rate constant for carbenium formation and k_3 is the rate constant for nucleophilic attack by NH_3 to form a *tert*-butylammonium ion.

Scheme 2. Mechanism of Isobutene Formation over MFI

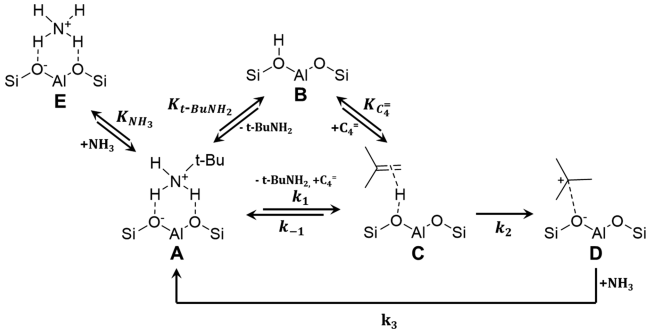

Taking adsorbed *t*-$BuNH_2$ to be the most abundant surface intermediate and carbenium formation to be the rate-limiting step, a rate expression can be obtained (eq 2).

$$r_{int} = \frac{K_1 k_2 [C_4^=]}{[t\text{-}BuNH_2]} \quad (2)$$

Here, K_1 represents the equilibrium constant for *t*-$BuNH_2$ desorption coupled with isobutene adsorption (k_1/k_{-1}), r_{int} represents the intrinsic reaction rate, and $[C_4^=]$ and $[t\text{-}BuNH_2]$ represent the local concentrations of isobutene and *t*-$BuNH_2$, respectively. The validity of the quasi-equilibrium assumption between states A and C is explored below. The final expression for the apparent rate is equivalent to that given in eq 1, defining $k_{app} = K_1 k_2$.

The form of this rate expression correctly predicts the dependences of the rate of isobutene amination on the partial pressures of isobutene, NH_3, and *t*-$BuNH_2$ (see Figures 6 and S8).

DFT Studies over MFI. QM/MM calculations on the H-MFI cluster show that *t*-$BuNH_2$ interacts strongly with the Brønsted proton and spontaneously forms the *tert*-butylammonium ion, which is stabilized by the strong electrostatic interactions with the framework. The heat of adsorption for *t*-$BuNH_2$ over MFI at 473 K ($\Delta H_{ads} = -189$ kJ mol^{-1}) is much larger than that of NH_3 ($\Delta H_{ads} = -132$ kJ mol^{-1}) or isobutene ($\Delta H_{ads} = -60$ kJ mol^{-1}). The relative order of adsorption strengths (*t*-$BuNH_2$ > NH_3 > $C_4^=$) is consistent with the FTIR spectra shown in 11. The change in enthalpy to form an adsorbed carbenium ion complex from gas-phase isobutene is −56 kJ mol^{-1}, suggesting little energetic penalty to form the intermediate species from the adsorbed π-complex.

The predicted free energy profile along the proposed reaction coordinate at 473 K is shown in Figure 13. The lowest free energy intermediate, adsorbed *t*-$BuNH_2$ (A), is designated as the resting state and is used as the reference state. Displacement of *t*-$BuNH_2$ by isobutene (C) comes at a free energy cost of 113 kJ mol^{-1}. An intermediate state for this assisted desorption step could not be determined accurately because of interactions between the bulky adsorbed complex and nearby framework atoms in the MM region. However, an upper bound on the free energy of activation was determined by modeling desorption as a stepwise mechanism, in which a vacant site (B) with gas-phase isobutene and *t*-$BuNH_2$ represents the highest free energy intermediate (124 kJ mol^{-1}). The subsequent activation of isobutene to form the carbenium ion has a free energy barrier of 131 kJ mol^{-1} relative to the resting state. This barrier represents the free energy maximum of the cycle and constitutes the rate-limiting step, as previously suggested by our rate measurements. Nucleophilic attack of NH_3 to the center of the carbenium ion is barrierless and downhill by 97 kJ mol^{-1}, in agreement with our determination of the reaction kinetics, which show that NH_3 is not involved in the rate-limiting step.

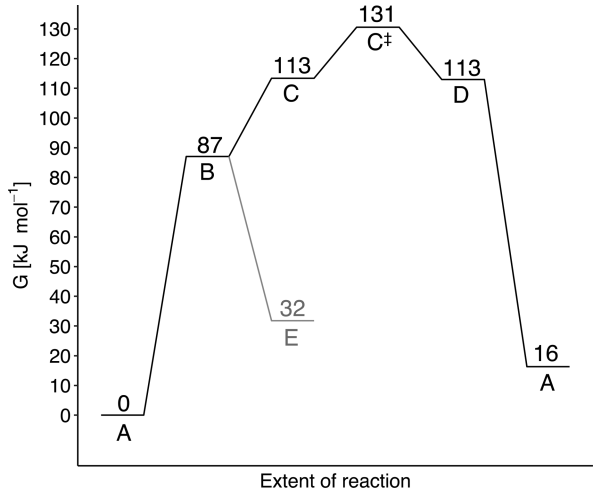

Figure 13. Predicted free energy profile of the amination of isobutene. T = 473 K and P = 1 atm. Intermediate states are labeled according to Scheme 2. The transition state for carbenium formation is denoted by C‡.

The associated enthalpy profile for the reaction is shown in Figure 14. The highest energy state (C‡) represents the kinetic barrier of the cycle. This suggests that the apparent activation enthalpy should be 143 kJ mol^{-1} relative to the resting state. Comparison of this value with the apparent activation barrier of around 180 kJ mol^{-1} measured for H-MFI raises the question about whether the assumption of pseudoequilibration between gas-phase and adsorbed *t*-$BuNH_2$ is correct throughout the reactor.

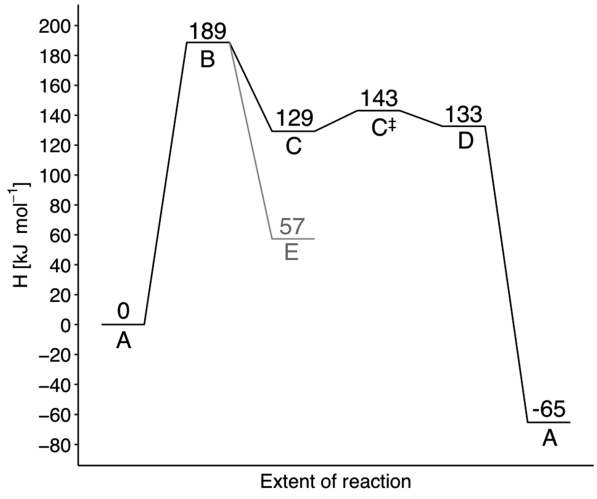

Figure 14. Predicted enthalpy profile of the amination of isobutene. T = 473 K; P = 1 atm. Intermediate states are labeled according to Scheme 2. The transition state of carbenium formation is denoted by C‡.

For the next stage of our analysis of the reaction kinetics, we determined the TOF for isobutene amination using the relationship developed by Kozuch and Shaik[26] (see eq S1), which accounts for the partial pressures of all reactants and products and makes no assumptions about the resting state of the catalyst. The resulting analysis leads to Figure 15, which

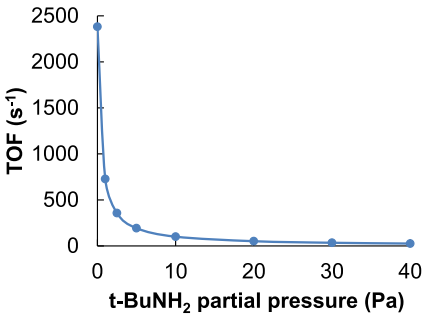

Figure 15. Predicted effect of *t*-$BuNH_2$ partial pressure on turnover frequency. T = 473 K; $P_{C_4^=}$ = 32 kPa; P_{NH_3} = 69 kPa.

shows that a fixed temperature and partial pressure of reactants, the TOF depends strongly on the partial pressure of *t*-$BuNH_2$. An Arrhenius analysis of the dependence of the TOF (see Figure S7) shows that the apparent activation energy is also sensitive to the partial pressure of *t*-$BuNH_2$. As seen in Figure 16, for very low *t*-$BuNH_2$ partial pressures, the apparent

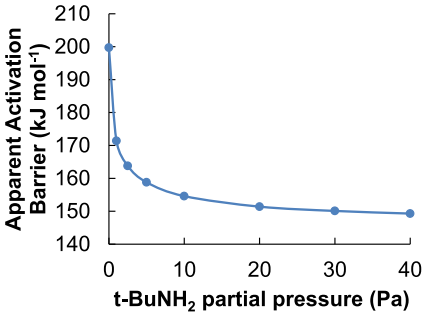

Figure 16. Predicted effect of *t*-$BuNH_2$ partial pressure on apparent activation barrier. T = 473 K; $P_{C_4^=}$ = 32 kPa; P_{NH_3} = 69 kPa.

activation energy is 200 kJ mol^{-1} and then decreases rapidly to below 150 kJ mol^{-1} for *t*-$BuNH_2$ partial pressures of order 40 Pa, which are typical of the highest values observed in our experiments. The results shown in Figures 15 and 16 suggest that *t*-$BuNH_2$ forms very rapidly in the initial part of the catalyst bed, where the partial pressure of *t*-$BuNH_2$ is very small, and then decreases rapidly with increasing bed length due to *t*-$BuNH_2$ inhibition. This would then explain why the measured apparent *t*-$BuNH_2$, 180 kJ mol^{-1}, lies closer to the upper end of the values reported in Figure 16.

We obtained further insights into the kinetics from an analysis of the degree of TOF control as a function of *t*-$BuNH_2$ partial pressure. This analysis revealed that for very low *t*-$BuNH_2$ partial pressures, there is not enough gas-phase *t*-$BuNH_2$ to displace adsorbed isobutene (C → A in Scheme 2). As a result, the assisted desorption of *t*-$BuNH_2$ is irreversible and rate limiting. However, as *t*-$BuNH_2$ partial pressures increase, displacement of adsorbed isobutene by gas-phase *t*-$BuNH_2$ becomes significant, which lowers the surface concentration of isobutene, and hence a lower rate of isobutene activation to the carbenium ion. At high enough *t*-$BuNH_2$ partial pressures, the pseudoequilibrium approximation for the assisted desorption of *t*-$BuNH_2$ becomes valid and the subsequent isobutene activation step becomes rate limiting. To summarize, the differences in the reaction mechanism at the inlet and outlet of the reactor are due to changes in the concentrations of gas-phase *t*-$BuNH_2$ and adsorbed isobutene. These limits can be represented by a pseudo steady-state rate expression given by eq 3, which captures the kinetic relevance of both *t*-$BuNH_2$ desorption and isobutene activation and explains the difference between the predicted and measured activation energies.

$$r_{int} = \frac{k_1 k_2 [C_4^=]}{k_{-1}[t\text{-BuNH}_2] + k_2} \tag{3}$$

The dominant term in eq 3 at the front end of the catalyst bed ($k_{-1}[t\text{-BuNH}_2] \ll k_2$) is desorption of *t*-$BuNH_2$, characterized by k_1, while at the outlet ($k_{-1}[t\text{-BuNH}_2] \gg k_2$), the dominant term becomes the activation of isobutene, characterized by $K_1 k_2$. Therefore, the true apparent activation barrier represents a weighted average of enthalpies between states B and $C^{\ddagger}$.

CONCLUSIONS

A combined experimental and theoretical study was performed to gain insights into the mechanism and kinetics of isobutene amination over zeolites. The active sites are Brønsted acidic protons located within the zeolites pores. Small-pored zeolites with one-dimensional channels are inactive because *t*-$BuNH_2$ blocks the pore mouths and impedes diffusion of isobutene. However, if the pore size is larger than a critical diameter, the intrinsic rate and activation energy become invariant with zeolite topology. FTIR and TPD studies reveal that *t*-$BuNH_2$ strongly inhibits the active site, although *t*-$BuNH_2$ desorption can be assisted by the concurrent adsorption of isobutene. Isobutene is protonated in the rate-limiting step to form the carbenium intermediate, which immediately couples to form *t*-$BuNH_2$. However, at very low *t*-$BuNH_2$ partial pressures, such as at the inlet to the reactor, the rate-limiting step switches to *t*-$BuNH_2$ desorption. The proposed mechanism shows excellent agreement with experimental rate data and is consistent with results obtained from DFT simulations.

AUTHOR INFORMATION

Corresponding Author

*E-mail: alexbell@berkeley.edu.

ORCID

Martin Head-Gordon: 0000-0002-4309-6669

Alexis T. Bell: 0000-0002-5738-4645

Author Contributions

[⊥]C.R.H. and L.A.B. contributed equally.

Notes

The authors declare no competing financial interest.

■ ACKNOWLEDGMENTS

This work was funded by Director, Office of Science, Office of Basic Energy Sciences of the U.S. Department of Energy under Contract No. DE-AC02-05CH11231. DFT Calculations were performed on a computing cluster sponsored by the National Institutes of Health (NIH S10OD023532). The authors would like to thank Jeroen Van der Mynsbrugge, Neelay Phadke, and Julie Rorrer for helpful discussions.

■ REFERENCES

(1) Müller, T. E.; Hultzsch, K. C.; Yus, M.; Foubelo, F.; Tada, M. Hydroamination: Direct Addition of Amines to Alkenes and Alkynes. *Chem. Rev.* **2008**, *108*, 3795−3892.

(2) Hölderich, W. F.; Heitmann, G. Synthesis of Intermediate and Fine Chemicals on Heterogeneous Catalysts with Respect to Environmental Protection. *Catal. Today* **1997**, *38*, 227−233.

(3) Taglieber, V.; Hoelderich, W.; Kummer, R.; Mross, W. D.; Saladin, G. Preparation of Tert-Butylamine from Isobutene. U.S. Patent 4,929,758, 1990.

(4) Taglieber, V.; Hoelderich, W.; Kummer, R.; Mross, W. D.; Saladin, G. Production of Amines from an Olefin and Ammonia or a Primary or Secondary Amine. U.S. Patent 4,929,759, 1990.

(5) Gao, S.; Zhu, X.; Li, X.; Wang, Y.; Zhang, Y.; Xie, S.; An, J.; Chen, F.; Liu, S.; Xu, L. Thermodynamic Study of Direct Amination of Isobutylene to Tert-Butylamine. *Chin. J. Catal.* **2017**, *38*, 106−114.

(6) Lequitte, M.; Figueras, F.; Moreau, C.; Hub, S. Amination of Butenes over Protonic Zeolites. *J. Catal.* **1996**, *163*, 255−261.

(7) Deeba, M.; Ford, M. E.; Johnson, T. a. Direct Amination of Ethylene by Zeolite Catalysis. *J. Chem. Soc., Chem. Commun.* **1987**, No. 8, 562.

(8) Deeba, M.; Ford, M. E. Heterogeneous Acid-Catalyzed Amination of Isobutene to Tert-Butylamine. *J. Org. Chem.* **1988**, *53*, 4594−4596.

(9) Deeba, M.; Ford, M. E. Direct Amination of Olefins: A Comparative Study over Erionite and Y Zeolites. *Zeolites* **1990**, *10*, 794−797.

(10) Mizuno, N.; Tabata, M.; Uematsu, T.; Iwamoto, M. Amination of 2-Methylpropene over Proton-Exchanged ZSM-5 Zeolite Catalysts. *J. Catal.* **1994**, *146*, 249−256.

(11) Chen, D.; Zhang, L.; Yi, C.; Dumesic, J. Methylamine Synthesis over Solid Acid Catalysts: Microcalorimetric and Infrared Spectroscopic Studies of Adsorbed Species. *J. Catal.* **1994**, *146*, 257−267.

(12) Gayubo, A. G.; Benito, P. L.; Aguayo, A. T.; Olazar, M.; Bilbao, J. Relationship between Surface Acidity and Activity of Catalysts in the Transforhation of Methanol into Hydrocarbons. *J. Chem. Technol. Biotechnol.* **1996**, *65*, 186−192.

(13) Parrillo, D. J.; Gorte, R. J. Characterization of Acidity in H-ZSM-5, H-ZSM-12, H-Mordenite, and H-Y Using Microcalorimetry. *J. Phys. Chem.* **1993**, *97*, 8786−8792.

(14) Parrillo, D. J.; Gorte, R. J.; Farneth, W. E. A Calorimetric Study of Simple Bases in H-ZSM-5: A Comparison with Gas-Phase and Solution-Phase Acidities. *J. Am. Chem. Soc.* **1993**, *115*, 12441−12445.

(15) Gründling, C.; Eder-Mirth, G.; Lercher, J. Surface Species in the Direct Amination of Methanol Over Brønsted Acidic Mordenite Catalysts. *Res. Chem. Intermed.* **1997**, *23*, 25−40.

(16) Veefkind, V. A.; Lercher, J. A. On the Elementary Steps of Acid Zeolite Catalyzed Animation of Light Alcohols. *Appl. Catal., A* **1999**, *181*, 245−255.

(17) Parrillo, D. J.; Adamo, a. T.; Kokotailo, G. T.; Gorte, R. J. Amine Adsorption in H-ZSM-5. *Appl. Catal.* **1990**, *67*, 107−118.

(18) Palkhiwala, A. G.; Gorte, R. J. Characterization of H-FER and H-TON Using Temperature-Programmed Desorption of Alkylamines. *Catal. Lett.* **1999**, *57*, 19−23.

(19) Gao, S.; Zhu, X.; Li, X.; Wang, Y.; Xie, S.; Du, S.; Chen, F.; Zeng, P.; Liu, S.; Xu, L. Direct Amination of Isobutylene over Zeolite Catalysts with Various Topologies and Acidities. *J. Energy Chem.* **2017**, *26*, 776−782.

(20) Janda, A.; Vlaisavljevich, B.; Lin, L. C.; Smit, B.; Bell, A. T. Effects of Zeolite Structural Confinement on Adsorption Thermodynamics and Reaction Kinetics for Monomolecular Cracking and Dehydrogenation of N-Butane. *J. Am. Chem. Soc.* **2016**, *138*, 4739−4756.

(21) Zimmerman, P. M.; Head-Gordon, M.; Bell, A. T. Selection and Validation of Charge and Lennard-Jones Parameters for QM/MM Simulations of Hydrocarbon Interactions with Zeolites. *J. Chem. Theory Comput.* **2011**, *7*, 1695−1703.

(22) Li, Y.-P.; Gomes, J.; Mallikarjun Sharada, S.; Bell, A. T.; Head-Gordon, M. Improved Force-Field Parameters for QM/MM Simulations of the Energies of Adsorption for Molecules in Zeolites and a Free Rotor Correction to the Rigid Rotor Harmonic Oscillator Model for Adsorption Enthalpies. *J. Phys. Chem. C* **2015**, *119*, 1840−1850.

(23) Vanommeslaeghe, E.; Hatcher, E.; Acharya, C.; Kundu, S.; Zhong, S.; Shim, J.; Darian, E.; Guvench, O.; Lopes, P.; Vorobyov, I.; Mackerell, A. D., Jr. CHARMM General Force Field: A Force Field for Drug-Like Molecules Compatible with the CHARMM All-Atom Additive Biological Force Fields. *J. Comput. Chem.* **2010**, *31*, 671−690.

(24) Grimme, S. Supramolecular Binding Thermodynamics by Dispersion-Corrected Density Functional Theory. *Chem. - Eur. J.* **2012**, *18*, 9955−9964.

(25) Shao, Y.; Gan, Z.; Epifanovsky, E.; Gilbert, A. T. B.; Wormit, M.; Kussmann, J.; Lange, A. W.; Behn, A.; Deng, J.; Feng, X.; Ghosh, D.; Goldey, M.; Horn, P. R.; Jacobson, L. D.; Kaliman, I.; Khaliullin, R. Z.; Kuś, T.; Landau, A.; Liu, J.; Proynov, E. I.; Rhee, Y. M.; Richard, R. M.; Rohrdanz, M. a.; Steele, R. P.; Sundstrom, E. J.; Woodcock, H. L.; Zimmerman, P. M.; Zuev, D.; Albrecht, B.; Alguire, E.; Austin, B.; Beran, G. J. O.; Bernard, Y. a.; Berquist, E.; Brandhorst, K.; Bravaya, K. B.; Brown, S. T.; Casanova, D.; Chang, C. M.; Chen, Y.; Chien, S. H.; Closser, K. D.; Crittenden, D. L.; Diedenhofen, M.; Distasio, R. a.; Do, H.; Dutoi, A. D.; Edgar, R. G.; Fatehi, S.; Fusti-Molnar, L.; Ghysels, A.; Golubeva-Zadorozhnaya, A.; Gomes, J.; Hanson-Heine, M. W. D.; Harbach, P. H. P.; Hauser, A. W.; Hohenstein, E. G.; Holden, Z. C.; Jagau, T. C.; Ji, H.; Kaduk, B.; Khistyaev, K.; Kim, J.; Kim, J.; King, R. a.; Klunzinger, P.; Kosenkov, D.; Kowalczyk, T.; Krauter, C. M.; Lao, K. U.; Laurent, A. D.; Lawler, K. V.; Levchenko, S. V.; Lin, C. Y.; Liu, F.; Livshits, E.; Lochan, R. C.; Luenser, A.; Manohar, P.; Manzer, S. F.; Mao, S. P.; Mardirossian, N.; Marenich, A. V.; Maurer, S. a.; Mayhall, N. J.; Neuscamman, E.; Oana, C. M.; Olivares-Amaya, R.; O'Neill, D. P.; Parkhill, J. a.; Perrine, T. M.; Peverati, R.; Prociuk, A.; Rehn, D. R.; Rosta, E.; Russ, N. J.; Sharada, S. M.; Sharma, S.; Small, D. W.; Sodt, A.; Stein, T.; Stück, D.; Su, Y. C.; Thom, A. J. W.; Tsuchimochi, T.; Vanovschi, V.; Vogt, L.; Vydrov, O.; Wang, T.; Watson, M. a.; Wenzel, J.; White, A.; Williams, C. F.; Yang, J.; Yeganeh, S.; Yost, S. R.; You, Z. Q.; Zhang, I. Y.; Zhang, X.; Zhao, Y.; Brooks, B. R.; Chan, G. K. L.; Chipman, D. M.; Cramer, C. J.; Goddard, W. a.; Gordon, M. S.; Hehre, W. J.; Klamt, A.; Schaefer, H. F.; Schmidt, M. W.; Sherrill, C. D.; Truhlar, D. G.; Warshel, A.; Xu, X.; Aspuru-Guzik, A.; Baer, R.; Bell, A. T.; Besley, N. a.; Chai, J. Da; Dreuw, A.; Dunietz, B. D.; Furlani, T. R.; Gwaltney, S. R.; Hsu, C. P.; Jung, Y.; Kong, J.; Lambrecht, D. S.; Liang, W.; Ochsenfeld, C.; Rassolov, V. a.; Slipchenko, L. V.; Subotnik, J. E.; Van Voorhis, T.; Herbert, J. M.; Krylov, A. I.; Gill, P. M. W.; Head-Gordon, M. Advances in Molecular Quantum Chemistry Contained in the Q-Chem 4 Program Package. *Mol. Phys.* **2015**, *113*, 184−215.

(26) Kozuch, S. A Refinement of Everyday Thinking: The Energetic Span Model for Kinetic Assessment of Catalytic Cycles. *WIREs Comput. Mol. Sci.* **2012**, *2*, 795−815.

(27) Celik, F. E.; Kim, T.-J.; Bell, A. T. Vapor-Phase Carbonylation of Dimethoxymethane over H-Faujasite. *Angew. Chem., Int. Ed.* **2009**, *48*, 4813−4815.

(28) Malysheva, L. V.; Paukshtis, E. A.; Kotsarenko, N. S. Mechanism of Deamination of Butylamines on Protonic Centers of HNaY Zeolite. *J. Catal.* **1987**, *104*, 31−36.

(29) Foster, M. D.; Rivin, I.; Treacy, M. M. J.; Delgado Friedrichs, O. A Geometric Solution to the Largest-Free-Sphere Problem in Zeolite Frameworks. *Microporous Mesoporous Mater.* **2006**, *90*, 32−38.
(30) Natal-Santiago, M. A.; Dumesic, J. A. Microcalorimetric, FTIR, and DFT Studies of the Adsorption of Methanol, Ethanol, and 2,2,2-Trifluoroethanol on Silica. *J. Catal.* **1998**, *175*, 252−268.
(31) Lequitte, M.; Figueras, F.; Moreau, C.; Hub, S. Deamination of Sec-Butylamine over Acidic Zeolites. *Appl. Catal., A* **1992**, *84*, 155−168.
(32) Malysheva, L. V.; Paukshtis, E. A.; Kotsarenko, N. S. Deamination of Butylamines on the Surface of Acidic Oxide Catalysts. *React. Kinet. Catal. Lett.* **1984**, *24*, 91−95.
(33) Di Iorio, J. R.; Bates, S. A.; Verma, A. A.; Delgass, W. N.; Ribeiro, F. H.; Miller, J. T.; Gounder, R. The Dynamic Nature of Brønsted Acid Sites in Cu−Zeolites During NOx Selective Catalytic Reduction: Quantification by Gas-Phase Ammonia Titration. *Top. Catal.* **2015**, *58*, 424−434.
(34) Phadke, N. M.; Van Der Mynsbrugge, J.; Mansoor, E.; Getsoian, A. B.; Head-Gordon, M.; Bell, A. T. Characterization of Isolated Ga3+ Cations in Ga/H-MFI Prepared by Vapor-Phase Exchange of H-MFI Zeolite with GaCl3. *ACS Catal.* **2018**, *8*, 6106−6126.
(35) Miessner, H.; Kosslick, H.; Lohse, U.; Parlitz, B.; Tuan, V. A. Characterization of Highly Dealuminated Faujasite-Type Zeolites: Ultrastable Zeolite Y and ZSM-20. *J. Phys. Chem.* **1993**, *97*, 9741−9748.
(36) Demmin, R. A.; Gorte, R. J. Design Parameters for Temperature-Programmed Desorption from a Packed Bed. *J. Catal.* **1984**, *90*, 32−39.
(37) Janda, A.; Bell, A. T. Effects of Si/Al Ratio on the Distribution of Framework Al and on the Rates of Alkane Monomolecular Cracking and Dehydrogenation in H-MFI. *J. Am. Chem. Soc.* **2013**, *135*, 19193−19207.
(38) Gounder, R.; Iglesia, E. Catalytic Consequences of Spatial Constraints and Acid Site Location for Monomolecular Alkane Activation on Zeolites. *J. Am. Chem. Soc.* **2009**, *131*, 1958−1971.
(39) Dědeček, J.; Kaucký, D.; Wichterlová, B. Al Distribution in ZSM-5 Zeolites: An Experimental Study. *Chem. Commun.* **2001**, No. 11, 970−971.
(40) Sklenak, S.; Dědeček, J.; Li, C.; Wichterlová, B.; Gábová, V.; Sierka, M.; Sauer, J. Aluminum Siting in Silicon-Rich Zeolite Frameworks: A Combined High-Resolution 27Al NMR Spectroscopy and Quantum Mechanics/Molecular Mechanics Study of ZSM-5. *Angew. Chem., Int. Ed.* **2007**, *46*, 7286−7289.
(41) Cnudde, P.; De Wispelaere, K.; Van der Mynsbrugge, J.; Waroquier, M.; Van Speybroeck, V. Effect of Temperature and Branching on the Nature and Stability of Alkene Cracking Intermediates in H-ZSM-5. *J. Catal.* **2017**, *345*, 53−69.
(42) Song, W.; Nicholas, J. B.; Haw, J. F. Acid-Base Chemistry of a Carbenium Ion in a Zeolite under Equilibrium Conditions: Verification of a Theoretical Explanation of Carbenium Ion Stability. *J. Am. Chem. Soc.* **2001**, *123*, 121−129.